



Evaluation of polyvinyl toluene scintillators for fast neutron imaging

William C. Chuirazzi¹ · Ibrahim Oksuz¹ · Praneeth Kandlakunta¹ · Thomas N. Massey² · Carl R. Brune² · Nerine J. Cherepy³ · H. Paul Martinez³ · Lei Cao¹

Received: 26 April 2018 / Published online: 12 August 2018
© Akadémiai Kiadó, Budapest, Hungary 2018

Abstract

We evaluated polyvinyl toluene (PVT) scintillators fabricated with different emitting dopants and scintillator optical configurations for fast neutron imaging. A neutron imaging apparatus was constructed to study scintillators under MeV neutron exposure. PVT with 2% Xylol Flrpic emitter was identified as the brightest. The addition of a black backing to the scintillator, compared with a specular reflector film backing, improved the resolution of the neutron image obtained with the PVT scintillator by about 2 ×. It is concluded that a PVT imaging screen with 2% Xylol Flrpic, configured with a black backing, provides the best quality fast neutron image of the scintillators tested.

Keywords Neutron imaging · Fast neutron · Organic scintillator · PVT · Spatial resolution · Light yield

Introduction

Demands for international and domestic security over the last decades to detect explosives, weapons and contraband such as illegal substances or smuggled trade items have increased efforts to develop non-destructive screening technologies. A host of nondestructive testing methods including colorimetry, electrochemistry, ion detection spectroscopy, mass spectroscopy, x-ray spectroscopy, and x-ray imaging, amongst others [1, 2] are currently applied with varying degrees of effectiveness, time efficiency, and field deployability. Neutron imaging is one unique tool that augments current detection or inspection capabilities owing to the favorable properties of neutrons. Advantages of neutrons for non-destructive screening are their high penetration power in heavily shielded articles, their immunity from electromagnetic interference, and their ability to

discriminate between different materials of widely changing densities [3–5]. These characteristics also make neutron radiography well-suited for the examination of irradiated nuclear fuel, amongst other nuclear power applications [6–9]. Neutron tomography has recently been used to create a three-dimensional image of irradiated nuclear fuels [10–12]. The three-dimensional image produced by neutron tomography provides a powerful tool to analyze structural integrity of nuclear fuel during the post irradiation examination process.

Thermal neutron imaging has been explored extensively in the past [13–19]. However, thermal neutrons are not highly penetrating and are mainly useful for characterizing materials with strong thermal neutron capture cross sections. Additionally, thermal neutrons present concerns of activation and transmutation. Advantages of fast neutrons are their high penetration into dense materials and/or their mixtures with decreased activation concerns. Neutron generators, which typically produce fast neutrons through a fusion reaction, offer the added advantage of safety, as they can be switched on or off in a “turn-key” mode [20]. It is noted that the fast-neutron capture cross sections are low for most materials, helpful for preventing activation but also creating the need for a neutron imager with an increased efficiency. Fast neutrons impart more energy to lighter elements in elastic collisions, making them most suitable for detection and measurement applications involving lighter elements such as hydrogen (H) and

✉ Lei Cao
Cao.152@osu.edu

¹ Nuclear Engineering Program, Department of Mechanical and Aerospace Engineering, The Ohio State University, Columbus, OH 43210, USA

² Edwards Accelerator Laboratory, Department of Physics and Astronomy, Ohio University, Athens, OH 45701, USA

³ Lawrence Livermore National Laboratory, Livermore, CA 94550, USA

carbon (C). Light output and spatial resolution are the two most important performance parameters for neutron radiography using scintillation detectors [21]. Any fast neutron scintillation detector must be able to efficiently produce visible photons under neutron exposure while allowing those photons to escape the scintillator without a significant self-absorption.

Proton recoil is the mechanism that excites electrons and produces scintillation in plastic scintillators. In this effort, a neutron source with an average energy of 1.7 MeV and a maximum neutron energy of 3.2 MeV was used in conjunction with a CCD camera-based imaging system to evaluate plastic scintillator imaging screens. The 1.7 MeV neutron scattering cross-section is about 3 barns for H and 2 barns for C, constituting a mean free path of approximately 3.88 cm in PVT [22]. When a fast neutron enters a plastic scintillator and undergoes an elastic collision with H, or other light element's nucleus, part of the neutron energy is transferred to the nucleus. In polyvinyl toluene (PVT), the range of a recoiled proton, assuming maximum energy of 3.2 MeV, is 157 μm , which defines the theoretical resolution limit. The recoil nucleus travels through the scintillation material, exciting electrons. Once these electrons de-excite, photons are released, creating scintillation light. The number of photons emitted in the scintillation process is proportional to the number of incident neutrons as well as the energy of the neutrons.

While high energy neutron imaging is being recognized for its potential applications, it has not yet been deployed widely [23–25], partially due to the low sensitivity of scintillating materials for fast neutron imaging. Research on fast-neutron plastic scintillation detector development [26, 27] aims to improve light yield, as well as optical configuration. The purpose of this study is to determine how various dopant emitters and the optics of the scintillator affect the light yield and resolution of PVT scintillators. Our goal is to develop a well-characterized fast neutron plastic scintillator offering the best combination of MeV neutron efficiency, light yield, and spatial resolution. In this paper, studies were performed using MeV neutrons produced at Ohio University's Edwards Accelerator in conjunction with an imaging apparatus constructed at The Ohio State University to test the scintillators manufactured at Lawrence Livermore National Laboratory.

Experimental

Scintillators

Ten different scintillator samples, all containing PVT mixed with various emitters, were measured under fast neutron irradiation. The samples were all 1.0 inch

(2.54 cm) in diameter and 2.4 mm thick. Photos of the scintillators are in Fig. 1 while a list of all the scintillators is summarized in Table 1. The first seven samples shown in the table, HPM 144 through HPM 187, are all PVT material, each with a different emitter. Among them, HPM 169 was doped with a Europium (Eu) metal organic emitter, HPM 186 with tetraphenyl butadiene (TPB) and HPM 187 with 4-methyl-7-diethylaminocoumarin (MDAC). These samples were all optically configured with a standard black film backing on one face of the scintillator. The purpose of testing these scintillators was to determine which emitters could improve the scintillators' light yield under fast neutron irradiation. Flrpic (Bis[2-(4,6-difluorophenyl)pyridinato-C₂,N](picolinato)iridium(III), used in HPM 144 and 184, has the chemical formula C₂₈H₁₆F₄IrN₃O₂. X-Flrpic, found in HPM 164 and 185, stands for Xylyl Flrpic, is a Flrpic derivatized with a Xylyl group to improve solubility and shift the emission wavelength to a deeper green color. The emitter doping levels in the PVT were between 1.0 and 2.0% because light yield increases dramatically until 1.0% and has a minor increase between 1.0 and 2.0%. The solubility limit is around 3%, limiting the highest achievable emitter concentration to 2.0% doping.

The other three samples, HPM 305, HPM 306 and HPM 307, were prepared after initial light yield testing had been conducted on HPM 144–187. HPM 305–HPM 307 were all loaded with 2% X-Flrpic emitter. Different image enhancement configurations were tested on these samples, allowing measurements to determine which backing gave the best combination of light yield and image spatial resolution. In addition to the black backing, a specular film, which was used to reflect light, as well as a phosphor film, were both utilized. Iikura et al. [28] have conducted previous studies of specular film's enhancement of light yield.

Neutron source

The Edwards Accelerator utilizes a 4.5 MV tandem Pelletron accelerator which supports high beam intensities. The facility can create neutron, proton, deuteron, helium, lithium, boron and carbon beams. The neutron sources, which can be either monoenergetic or "white," can cover the energy range from 0.5 MeV to 24 MeV [29, 30]. All neutron images for this study were obtained at the Edwards Accelerator Laboratory, which provides a relatively "clean" neutron beam with little gamma-ray contamination. For this experiment, a 5 MeV proton beam incident on a beryllium-9 (⁹Be) target was used to create a neutron beam through a (p, n) reaction. The spectrum of fast neutrons produced had an average energy of 1.7 MeV, a maximum energy of 3.2 MeV and ranged down into the thermal region. The spectrum contained two peaks,

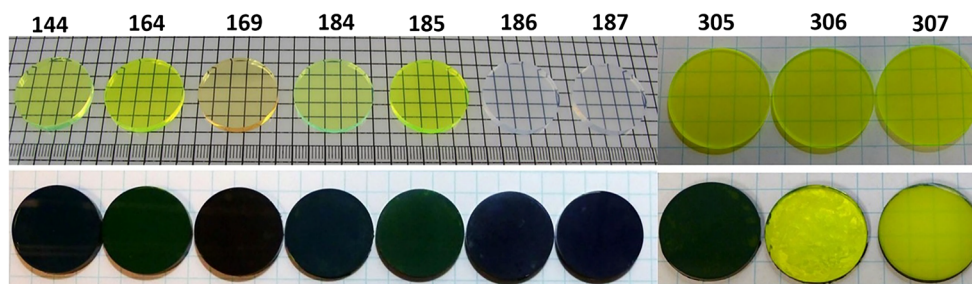


Fig. 1 Scintillator photographs. The top row shows the bare scintillators while the bottom row shows the scintillators with backings attached

Table 1 Scintillator dimensions, emitter dopants, and optical configurations

Scintillator I.D.	Emitter	Optical configuration
HPM 144	2% Flrpic	Black backing
HPM 164	2% X-Flrpic	Black backing
HPM 169	2% Eu	Black backing
HPM 184	1% Flrpic, 19% Bi	Black backing
HPM 185	2% X-Flrpic	Black backing
HPM 186	1.5% TPB	Black backing
HPM 187	1.5% MDAC	Black backing
HPM 305	2% X-Flrpic	Black backing
HPM 306	2% X-Flrpic	Specular reflector film
HPM 307	2% X-Flrpic	⁶ Li-ZnS:Cu phosphor paint

All scintillators have a diameter of 25.4 mm and a thickness of 2.4 mm

exhibiting its highest neutron yields at about 0.5 MeV and 2.75 MeV.

Neutron flux was calculated by measuring the charge accumulated from the proton beam before it interacted with the beryllium (Be) target and created the neutrons [31]. The beam angle was known to be 0°, allowing the neutron flux to be computed with the method described in Agosteo et al. [32]. The target was switched out during the experiment leading to two different neutron fluxes. Calibration showed the beam intensity to have an error of 5% [33]. When measuring the light yields of HPM 144–HPM 187, the average number of neutrons incident on the scintillators was $24,553 \pm 2455$ n/s. The light yield and resolution measurements for HPM 305–HPM 307 were taken with the scintillators exposed to an average number of neutrons of $55,548 \pm 5554$ n/s.

Minimization of the gamma-ray content in the neutron beam is important, as PVT is also sensitive to gamma rays. The gamma ray dose of the scintillators was measured to ensure that the scintillation comes primarily from the fast neutrons, and not the gamma rays. Gamma-ray contamination in the neutron beam was measured in two ways. The optically stimulated luminescence dosimeters (nanoDots™

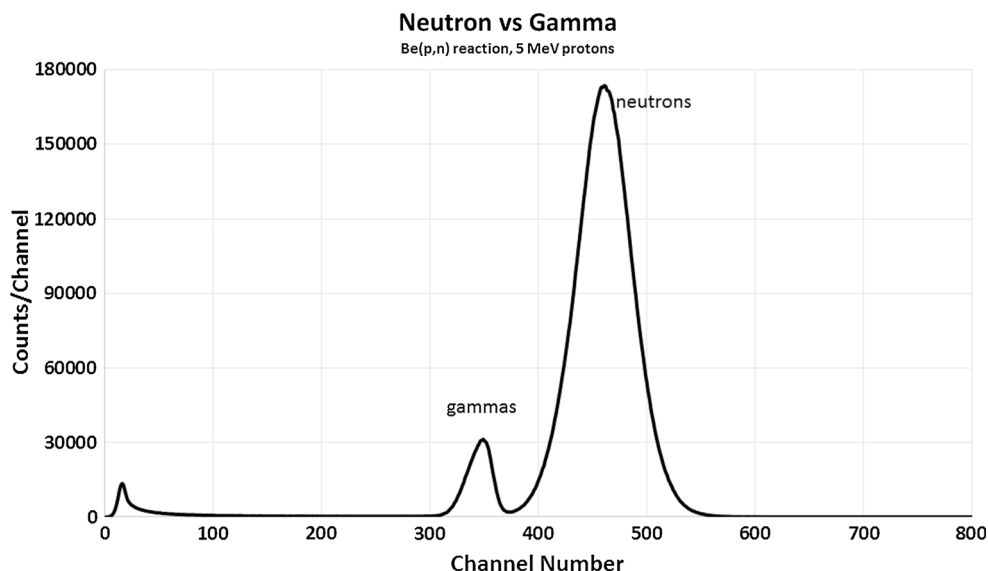
by Landauer) were used to measure the gamma-ray dose in the neutron beam [34]. The nanoDots, which measure the gamma dose over a 1 mm² area, measured an average gamma-ray dose rate of 500 ± 28 nGy/s when placed in the beam path, attached to the front of the imaging apparatus at a distance of 4 m away from the Be target.

The second method of measuring the gamma-ray content was by placing an NE-213 liquid scintillation detector, comprised of xylene, in the beam path and to determine the ratio of neutrons to gamma rays [35]. This detector was positioned about 2 m behind the location of the nanoDots. The detector indicated 12.6 neutrons per each gamma ray present. This result is shown in Fig. 2. Gamma-ray count rates were 1949 ± 194 γ/s and 4409 ± 409 γ/s, respectively, in the two different target configurations. The dose rate of 500 ± 28 nGy/s of the nanoDots is validated by the gamma-ray flux measured by the NE-213 detector after accounting for geometrical set-up, detector efficiency and gamma-ray energy. The discrepancy between the nanoDots and NE-213 detector measurements can be explained because the nanoDot's useful dose range is from 50 μGy to 1500 cGy. A reading of 500 nGy reading shows the gamma dose is below its detection limits, which also suggests a negligible amount of dose was collected.

Imaging apparatus

An electron-multiplying charge coupled device (EMCCD) camera [36] was used to capture the low-level lights from scintillator images. The sensitivity of the EMCCD was adjusted to compensate for the low light levels created by the scintillator because of the low interaction cross-section for fast neutrons. An electron multiplying gain of 150 was used to acquire images. Thermal noise was eliminated by keeping the camera temperature at a constant -69 °C using a 26.5 l cooling reservoir, with approximately 7.5 l consisting of ice and the other 19 l containing water. The camera cooling reservoir was used in conjunction with the camera's four-stage Peltier thermoelectric cooler to ensure temperature remained stable throughout the duration of the experiment.

Fig. 2 Neutron vs Gamma results from the NE-213 detector, primarily made of xylene, measured a 12.6:1 n:γ ratio



The EMCCD was enclosed in a light-tight box that was constructed from anodized aluminum to minimize delayed activation gamma photons under neutron irradiation. The box was covered in flat-black paint to prevent photons from reflecting inside the box and distorting the image. A duvetyne cloth, also known as a commando cloth, was also placed over the light-tight box during the experiment only as a precautionary step.

The scintillator was mounted inside the box and a front-surface mirror angled at 45° was used to reflect the image into the EMCCD lens. The camera was controlled remotely from the control room. A schematic diagram of

the set-up is shown in Fig. 3. Figure 4 shows the scintillator's position relative to the collimator in the beam path.

Data analysis

Two characteristics, light yield and resolution, were used to analyze the effectiveness of the scintillators. A relative light yield measurement was conducted to compare the effect of emitters on the photon output of the scintillators. Light yield was measured by taking an image of each scintillator and integrating the grayscale value of an area

Fig. 3 Schematic of experimental set-up. The scintillator is placed in the light-tight box and the imaging object is placed outside the box, between the neutron beam and the scintillator

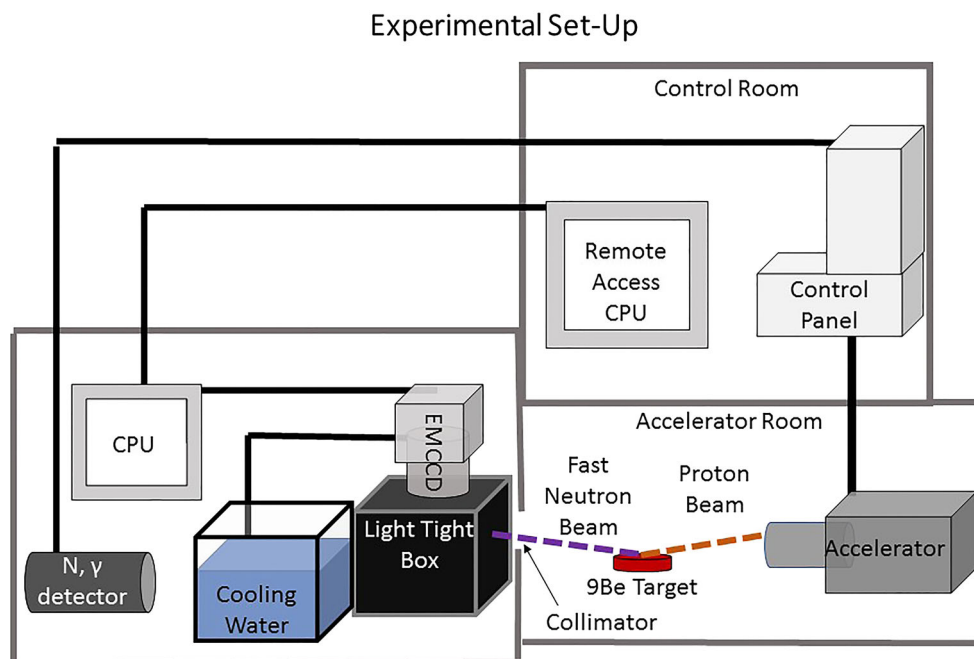
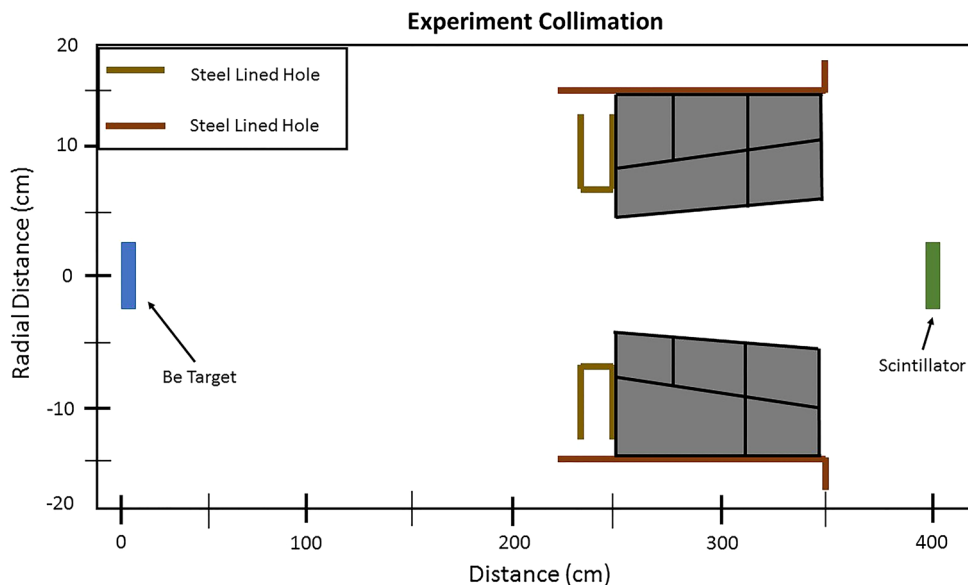


Fig. 4 Scintillator in beam path and beam collimation

inside the scintillator region. Background was accounted for by subtracting an integrated background gray value from the integrated scintillator gray scale value. The gray scale value is assumed to be proportional to the light intensity of the scintillator. These values were then normalized to the largest integrated grayscale value, allowing the scintillators to be compared relative to one another. The higher the relative light intensity, the greater the effect of emitter on increasing light yield.

Resolution was measured using the Modulation Transfer Function (MTF). The MTF was calculated by placing a neutron-attenuating object in the neutron beam, producing an edge in the image created by the scintillator. This edge was then measured to determine how well the scintillator could resolve the contrast between the light and dark edge. The spatial resolution is reported, in line pairs per mm (lp/mm), at 10% of the MTF.

Experimental uncertainties

Instrumental limitations led to uncertainties in the measured radiation dose as well as the light yield and MTF. Spatial resolution is limited by the 16 μm pixel size in the 512×512 pixel array of the EMCCD. Charge collection on the silicon chips also had some variance, resulting in a measured grayscale σ of 0.12% in the scintillator region of the images.

Degradation factors to the spatial resolution in the entire imaging chain, as well as the uncertainties of the MTF measurement, come from the neutron beam L/D ratio, divergence of the neutron beam (2.83°), neutron scattering, stray radiation, camera lens, mirror reflection, and finally the electronic noise. However, since relative comparisons are being made between the scintillators to determine the

optimum configuration, these errors should be uniform for all scintillators and can be cancelled out.

Results and discussion

Effect of emitters on scintillator light yields

Firstly, the scintillators with different emitters, HPM 144–HPM 187, were tested to determine which emitters produced the highest light yield. Image quality was determined by the exposure time and the electron multiplication (EM) gain. The images in Fig. 5 were taken with an EM gain of 150 and an exposure time of 20 min. These parameters were chosen as previous experiments determined this was the optimum combination when considering resolution, saturation and experimental time limits. Each scintillator was imaged with a neutron exposure of $24,553 \pm 2,4553$ n/s. After the images were obtained, a median filter with a radius of 6 pixels was applied and the contrast was adjusted to provide a picture optimized for viewing. The post-processed images are shown in Fig. 5, while the light yields resulting from these images are summarized in Table 2, where they are normalized to the scintillator producing the highest light yield, HPM 164. All images in Fig. 5 are shown at the same contrast level, meaning the brighter the image in the figure, the larger the number of photons produced by the scintillator. Uncertainty in the values is estimated at $\pm 15\%$, due to variations in the neutron flux and small changes in the geometry of the system between runs. The two samples with the highest photon production were HPM 164 and HPM 185, both of which contained the X-Flrpic emitter. A conventional formulation, similar to commercial plastic scintillator was used for HPM 186, which offers $\sim 2 \times$ lower light yield compared to HPM 164.

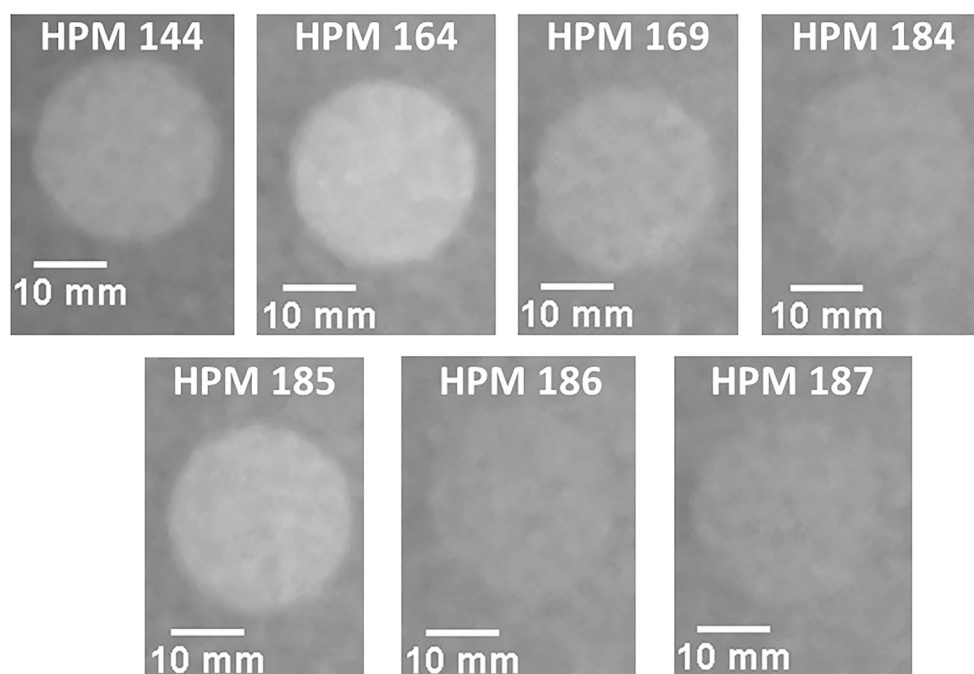


Fig. 5 Images showing light yields of scintillators, all images at the same contrast value

Table 2 Relative light yield results of PVT doped with various emitters

Scintillator I.D.	Emitter	Normalized light yield
HPM 144	2% Flrpic	0.78
HPM 164	2% X-Flrpic	1.00
HPM 169	2% Eu	0.70
HPM 184	1% Flrpic, 19% Bi	0.29
HPM 185	2% X-Flrpic	0.90
HPM 186	1.5% TPB	0.43
HPM 187	1.5% MDAC	0.47

Light yield and spatial resolution

After determining that doping PVT with 2% X-Flrpic emitter increased the light yield under fast neutron exposure, three 2% X-Flrpic PVT scintillators (HPM 305, 306 and 307) were prepared, each with a different optical configuration, such as (1) with a black backing film, (2) with specular reflector film, and (3) with luminescent and diffuse scattering ${}^6\text{Li-ZnS:Cu}$ phosphor paint, to determine which configuration would provide the highest light yield. Additionally, the spatial resolution of the scintillator samples was measured to find which configuration would give the best combination of light yield and spatial resolution.

An edge profile, necessary for calculating the MTF, was obtained using a high-density polyethylene (HDPE) block of dimensions 0.5 in \times 6 in \times 6 in (1.27 cm \times 15.24

cm \times 15.24 cm) to attenuate the neutrons. The darker areas on the scintillator in the neutron images correspond to the position of HDPE where neutrons were blocked from reaching the scintillator, thus avoiding the proton recoil collision and subsequent scintillation in the PVT material.

The light yield was calculated using the same method employed for HPM 144–HPM 187 scintillators, but the neutron beam delivered an average of $55,548 \pm 5554$ n/s and 4409 ± 440 γ /s to the scintillator samples. The same beam was used to acquire resolution measurements. The increased flux was caused by switching out one ${}^9\text{Be}$ target for another and tuning the beam.

Images used to obtain the edge profile and the MTF, are shown in Fig. 6. The images were acquired with an EM gain of 150 and an exposure time of 15 min. The shorter exposure time was due to the increased efficiency of HPM 305–307 when compared to HPM 144–187. The images were post-processed using white and dark noise filters of a 3-pixel radius and a median filter with a radius of 10 pixels. The images in Fig. 4 are all shown at different contrast levels as the scintillator with the phosphor paint configuration had a light yield ten times greater than the scintillator with the black backing, rendering the scintillator with the black backing configuration difficult to view at the same contrast as the other scintillators.

A plot of the MTF, used to determine the spatial resolution of a scintillator, is shown in Fig. 7. The resolution value is reported at 10% of the MTF, indicated by the dotted line in Fig. 7. The spatial frequency, reported in line

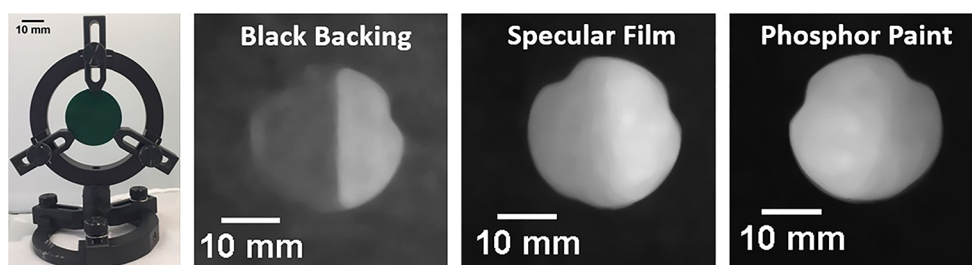


Fig. 6 Edge profile images used to calculate the MTF. Left image shows a real photo displaying the scintillator mounted on an optical stand. The mount affects the scintillator shape in the neutron images (right three images in the figure) for HPM 305, 306 and 307

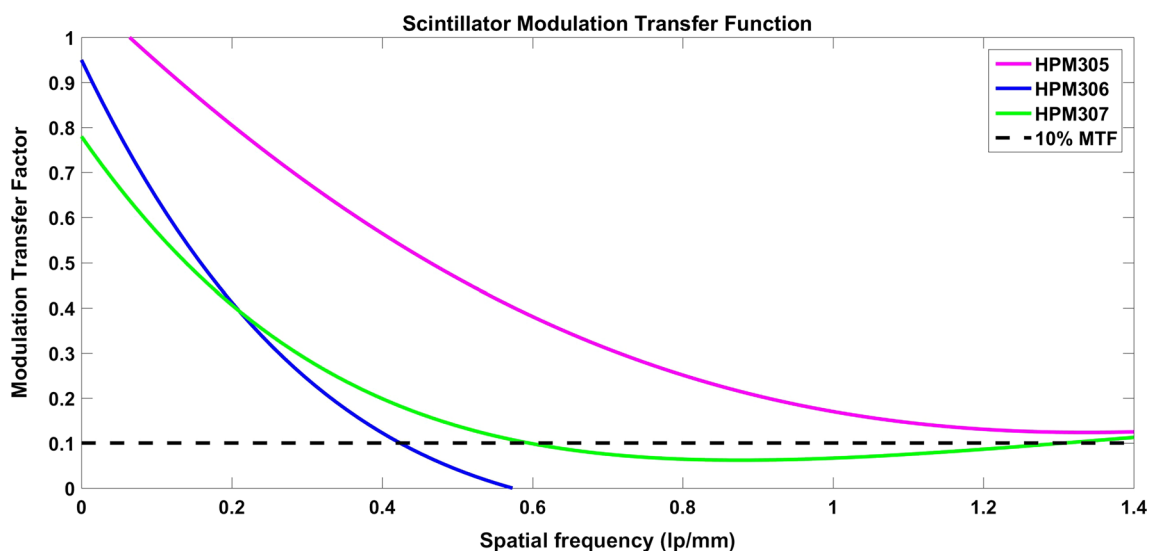


Fig. 7 The MTF plot, showing the resolution of scintillators

pairs per mm has been converted to a standard resolution measurement in units of millimeters in Table 3.

Table 3 details the different samples, their light yields and resolution obtained. While the phosphor paint increased the light yield of the scintillator by a factor of 5, this is mainly due to a thermal neutron capture by Lithium-6 in the phosphor paint, and therefore did not provide good high energy neutron imaging. The sensitivity to thermal neutrons disqualifies the scintillator with the phosphor paint from being a reliable fast-neutron imager. However, it may be possible that phosphor paint made without Li-6 could still be a viable alternative to increase light yield in fast neutron applications.

The specular reflector film redirected photons exiting the back of the scintillator to the front of the scintillator, allowing them to be captured by the EMCCD camera.

Adding the specular film to the scintillator increased the light yield compared to that of a scintillator with a black backing by about 120%. If photons created in the scintillator originate at different angles, the addition of specular film would be expected to increase the light yield as it reflects those photons which would be absorbed at the rear of a scintillator with a black backing.

The quantified light yield was also validated by attaching the scintillators to a quartz light pipe connected to a photomultiplier tube (PMT). In this case, the scintillator was placed in the beam path of a neutron beam facility at The Ohio State University Research Reactor (OSURR) with the PMT and a gamma spectroscopy system to measure the emitted photon spectrum. The OSURR, a pool-type research reactor utilizing uranium silicide (U_2Si_3) fuel plates, 19.8% enriched in ^{235}U fuel, operates up to a

Table 3 Relative light yields and resolution of PVT samples with different backings

Scintillator name	Image enhancement configuration	Normalized light yield	Resolution (mm)
HPM 305	Black backing	0.10	0.61
HPM 306	Specular film	0.22	1.35
HPM 307	Phosphor paint	1.00	0.82

licensed thermal power of 500 kW [18]. The neutron beam has a thermal equivalent flux of $1.27 \pm 0.03 \times 10^7$ n/(cm²s) at the end of the beam collimator when the reactor is operated at a power level of 450 kW [18]. While the OSURR supplied a primarily thermal neutron beam, its fast neutron contents helped to confirm the light yield trend observed under fast neutron irradiation. The thermal equivalent flux and fast neutron flux at the imaging location is measured at 4.4×10^6 n/(cm²s) and 4.4×10^4 n/(cm²s).

The black backing and specular film image enhancement configurations were tested in the OSURR thermal neutron beam. An image enhancement configuration of specular film increased the light yield of the scintillator by about 58% when compared with the scintillator with the black backing configuration. The difference in energies present in the fast and thermal neutron beams most likely accounts for the difference in light yield increase between the specular film and black backing configurations. Both tests confirm that the specular film offers a substantial increase in the light yield. While the addition of specular film increases light output, it degrades the imaging resolution of the PVT scintillator to about 45% of its resolution with a black backing. The decreased resolution occurs as the angle of reflection for the photons striking the specular film delocalizes the photons from their original position. When photons are displaced, the image becomes blurry, lowering the resolution offered by the scintillator.

HPM 305, which had the black backing image enhancement configuration, produced sufficient photons to allow for neutron imaging. The challenge with HPM 305, 306 and 307 was obtaining an image with an acceptable resolution. If spatial resolution is more critical to improving the imaging compared to the brightness, it is recommended to adopt the optical configuration using black backing for fast neutron imaging applications. It will be favorable, however, to use a specular backing in applications where the scintillator light yield is too low, overriding the need to have a higher spatial resolution.

Conclusions

In this study, we evaluated different plastic PVT scintillators for fast neutron imaging. Results from using various emitter dopants were compared to determine the optimal dopant in fast neutron scintillation applications. An X-Flrpic emitter, doped in PVT at 2% was found to increase the light yield in PVT by more than 2 × compared to traditional emitters used in plastic scintillators, such as TPB. This work shows that PVT with X-Flrpic emitters can be successfully utilized to increase photon production in PVT under fast-neutron irradiation.

Scintillator optical configurations were also explored to optimize fast neutron response of PVT scintillators. The specular reflector backing film was found to increase light yield by 2 × over that of a scintillator with a black backing configuration. However, the resolution with the specular film was degraded to about 1/2 that of the scintillator with black backing. In fast neutron imaging applications limited by low light yield, it is recommended to add a specular backing to increase the light yield, in order to enhance the image acquisition throughput. However, in scenarios with ample photon production, a black backing should be used to maximize the spatial resolution.

Additionally, fast neutron imaging could be conducted with PVT imaging screens of varied sizes to determine the size and optical magnification that produces the best fast neutron images. PVT doped with Iridium complex emitters have been demonstrated as a superior fast neutron imaging screen. Further studies to evaluate complex phantoms, shielding configurations, optimized optics, and imaging processing algorithms must be undertaken to realize the full potential of MeV neutron imaging.

Acknowledgements We would like to thank the financial support of Lawrence Livermore National lab and staff at The Ohio State University Nuclear Reactor Laboratory. The contributions of CB and TM were supported in part by the U.S. Department of Energy, under Grants No. DE-FG02-88ER40387 and DE-NA0002905.

References

1. Brown KE, Greenfield MT, McGrane SD, Moore DS (2016) Advances in explosives analysis—part I: animal, chemical, ion, and mechanical methods. *Anal Bioanal Chem* 408(1):35–47
2. Brown KE, Greenfield MT, McGrane SD, Moore DS (2016) Advances in explosives analysis—part II: photon and neutron methods. *Anal Bioanal Chem* 408(1):49–65
3. Whetstone ZD, Kearfott KJ (2014) A review of conventional explosives detection using active neutron interrogation. *J Radioanal Nucl Chem* 301(3):629–639
4. Buffler A, Tickner J (2010) Detecting contraband using neutrons: challenges and future directions. *Radiat Meas* 45(10):1186–1192
5. Buffler A (2004) Contraband detection with fast neutrons. *Radiat Phys Chem* 71(3):853–861
6. Craft AE, Wachs DM, Okuniewski MA, Chichester DL, Williams WJ, Papaioannou GC, Smolinski AT (2015) Neutron radiography of irradiated nuclear fuel at Idaho National Laboratory. *Phys Procedia* 69:483–490
7. Craft AE, Barton JP (2017) Applications of neutron radiography for the nuclear power industry. *Phys Procedia* 88:73–80
8. Groeschel F, Schleuniger P, Hermann A, Lehmann E, Wiesel L (1999) Neutron radiography of irradiated fuel rod segments at the SINQ: loading, transfer and irradiation concept. *Nucl Instrum Methods Phys Res Sect A* 424(1):215–220
9. Lehmann EH, Vontobel P, Hermann A (2003) Non-destructive analysis of nuclear fuel by means of thermal and cold neutrons. *Nucl Instrum Methods Phys Res Sect A* 515(3):745–759
10. Rai DK, Abir MI, Wu H, Khaykovich B, Moncton DE (2018) Focusing mirrors for enhanced neutron radiography with thermal

- neutrons and application for irradiated nuclear fuel. *Nucl Instrum Methods Phys Res Sect A* 879:141–146
11. Abir MI, Islam FF, Craft A, Williams WJ, Wachs DM, Chichester DL, Meyer MK, Lee HK (2016) Determination of optimal imaging parameters for the reconstruction of a nuclear fuel assembly using limited angle neutron tomography. *J Instrum* 11(01):C01016
 12. Abir MI, Islam FF, Wachs DM, Lee HK (2016) Sparse-view neutron CT reconstruction of irradiated fuel assembly using total variation minimization with Poisson statistics. *J Radioanal Nucl Chem* 307(3):1967–1979
 13. Cherepy NJ, Sanner RD, Beck PR, Swanberg EL, Tillotson TM, Payne SA, Hurlburt CR (2015) Bismuth-and lithium-loaded plastic scintillators for gamma and neutron detection. *Nucl Instrum Methods Phys Res Sect A* 778:126–132
 14. Ovechkina L, Riley K, Miller S, Bell Z, Nagarkar V (2009) Gadolinium loaded plastic scintillators for high efficiency neutron detection. *Phys Procedia* 2(2):161–170
 15. Katagiri M, Sakasai K, Matsubayashi M, Kojima T (2004) Neutron/ γ -ray discrimination characteristics of novel neutron scintillators. *Nucl Instrum Methods Phys Res Sect A* 529(1):317–320
 16. Brenizer JS, Berger H, Stebbings CT, Giles GT (1997) Performance characteristics of scintillators for use in an electronic neutron imaging system for neutron radiography. *Rev Sci Instrum* 68(9):3371–3379
 17. Turkoglu D, Cao L, Lewandowski R (2013) A low-cost neutron radiography device. *Phys Procedia* 43:54–65
 18. Lewandowski R, Cao L, Turkoglu D (2012) Noise evaluation of a digital neutron imaging device. *Nucl Instrum Methods Phys Res Sect A* 674:46–50
 19. Turkoglu D, Burke J, Lewandowski R, Cao L (2012) Characterization of a new external neutron beam facility at the Ohio State University. *J Radioanal Nucl Chem* 291(2):321–327
 20. Aleksandrov VD, Bogolubov EP, Bochkarev OV, Korytko LA, Nazarov VI, Polkanov YG, Ryzhkov VI, Khasaev TO (2005) Application of neutron generators for high explosives, toxic agents and fissile material detection. *Appl Radiat Isot* 63(5):537–543
 21. Milbrath BD, Peurrung AJ, Bliss M, Weber WJ (2008) Radiation detector materials: an overview. *J Mater Res* 23(10):2561–2581
 22. Harvey JA, Hill NW (1979) Scintillation detectors for neutron physics research. *Nucl Instrum Methods* 162(1-3):507–529
 23. Bogolubov E, Bugaenko O, Kuzin S, Mikerov V, Monitch E, Monitch A, Pertsov A (2015) CCD detectors for fast neutron radiography and tomography with a cone beam. *Nucl Instrum Methods Phys Res Sect A* 542(1-3):187–191
 24. Yang W, Bin T, Heyong H, Bin L, Ke T, Young S, Wei Y, Chao C (2013) The study of zinc sulphide scintillator for fast neutron radiography. *Phys Procedia* 43:205–215
 25. Nelson RO, Vogel SC, Hunter JF, Watkins EB, Losko AS, Tremsin AS, Borges NP, Cutler TE, Dickman LT, Espy MA, Gautier DC, Madden AC, Majewski J, Malone MW, Mayo DR, McClellan KJ, Montgomery DS, Mosby SM, Nelson AT, Ramos KJ, Schirato RC, Schroeder K, Sevanto SA, Swift AL, Vo LK, Williamson TE, Winch NM (2018) Neutron imaging at LANSCE—from cold to ultrafast. *J Imaging* 4(2):45
 26. Bravar U, Bruillard PJ, Flückiger EO, Macri JR, McConnell ML, Moser MR, Ryan JM, Woolf RS (2006) Design and testing of a position-sensitive plastic scintillator detector for fast neutron imaging. *IEEE Trans Nucl Sci* 53(6):3894–3903
 27. Dangendorf V, Kersten C, Laczko G, Vartsky D, Mor I, Goldberg MB, Feldman G, Breskin A, Chechik R, Jagutzky O, Spillman U (2004) Detectors for energy-resolved fast-neutron imaging. *Nucl Instrum Methods Phys Res Sect A* 535(1):93–97
 28. Iikura H, Tsutsui N, Saito Y, Nojima T, Yasuda R, Sakai T, Matsubayashi M (2013) Investigation of the brightness enhancement using brightness enhancement films on a scintillator. *Phys Procedia* 43:161–168
 29. Finlay RW, Brient CE, Carter DE, Marcinkowski A, Mellema S, Randers-Pehrson G, Rapaport J (1982) The Ohio University beam swinger facility. *Nucl Instrum Methods Phys Res* 198(2-3):197–206
 30. Meisel Z, Brune CR, Grimes SM, Ingram DC, Massey TN, Voinov AV (2017) The Edwards Accelerator at Ohio University. *Phys Procedia* 90:448–454
 31. Howard WB, Grimes SM, Massey TN, Al-Quraishi SI, Jacobs DK, Brient CE, Yanch JC (2001) Measurement of the thick-target ^9Be (p, n) neutron energy spectra. *Nucl Sci Eng* 138(2):145–160
 32. Agosteo S, Colautti P, Esposito J, Fazzi A, Intorini MV, Pola A (2011) Characterization of the energy distribution of neutrons generated by 5 MeV protons on a thick beryllium target at different emission angles. *Appl Radiat Isot* 69(12):1664–1667
 33. Massey TN, Al-Quraishi S, Brient CE, Guillemette JF, Grimes SM, Jacobs D, O'Donnell JE, Oldendick J, Wheeler R (1998) A measurement of the ^{27}Al (d, n) spectrum for use in neutron detector calibration. *Nucl Sci Eng* 129(2):175–179
 34. McKeever SW (2001) Optically stimulated luminescence dosimetry. *Nucl Instrum Methods Phys Res Sect B* 184(1):29–54
 35. Lurie NA, Harris L, Young JC (1975) Calculation of gamma-ray response matrix for 5 cm NE-213 organic liquid scintillation detector. *Nucl Instrum Methods* 129(2):543–555
 36. Robbins MS, Hadwen BJ (2003) The noise performance of electron multiplying charge-coupled devices. *IEEE Trans Electron Devices* 50(5):1227–1232